Pharmaceutical Research, Vol. 25, No. 10, October 2008 (© 2008)
DOI: 10.1007/s11095-008-9612-5

Research Paper

Decreased Lithium Disposition to Cerebrospinal Fluid in Rats with Glycerol-induced Acute Renal Failure

Rie Sakae,[1] Atsuko Ishikawa,[1] Tomoko Niso,[1] Yukiko Komori,[1] Tetsuya Aiba,[1,2] Hiromu Kawasaki,[1] and Yuji Kurosaki[1]

Received February 21, 2008; accepted April 25, 2008; published online June 26, 2008

Purpose. The lithium disposition to cerebrospinal fluid (CSF) was evaluated in rats with acute renal failure (ARF) to examine whether electrolyte homeostasis of the CSF is perturbed by kidney dysfunction. In addition, the effects of renal failure on choroid plexial expressions of the Na^+–K^+–$2Cl^-$ co-transporter (NKCC1) and Na^+/H^+ exchanger (NHE1) were also studied.
Methods. After lithium was intravenously administered at a dose of 4 mmol/kg, its concentration profile in plasma was evaluated by collecting plasma specimens, while that in CSF was monitored with a microdialysis probe in the lateral ventricles. NKCC1 and NHE1 expressions were measured via the Western immunoblot method using membrane specimens prepared from the choroid plexus in normal and ARF rats.
Results. The lithium concentration in CSF of ARF rats was 30% lower than that of normal rats, while their plasma lithium profiles were almost the same, indicating that the lithium disposition to CSF was decreased in ARF rats. It was revealed that the choroid plexial expression of NKCC1 was increased by 40% in ARF rats, but that of NHE1 was unchanged.
Conclusion. ARF decreases the lithium disposition to CSF, possibly by promoting lithium efflux from CSF due to increased NKCC1 expression in the choroid plexus.

KEY WORDS: acute renal failure; cerebrospinal fluid (CSF); choroid plexus; lithium; Na^+–K^+–$2Cl^-$ co-transporter (NKCC1).

INTRODUCTION

It is well-known that decreased renal function can be life-threatening. This is largely because the kidney plays an important role in maintaining homeostasis by performing various essential functions. It is reported that the kidney regulates the body's content of water and electrolytes via reabsorption and excretion processes mediated by channels and transporters expressed in the renal tubule epithelia, such as the amirolide-sensitive Na^+ channel, Na^+–K^+–$2Cl^-$ co-transporter, and Na^+/H^+ exchanger (1–4).

As the kidney is crucial for maintaining homeostasis, it is understandable that renal failure affects other organs, altering their functions. In fact, it was demonstrated that the hepatic function of metabolizing therapeutic compounds is changed in rats with experimental renal failure, markedly altering their pharmacokinetics (5,6). In the intestine, the barrier function preventing xenobiotic absorption is decreased in renal failure, resulting in an increase in their intestinal absorption (7,8). These functional changes of the liver and intestine seem to be related to the fact that the expressions of drug-metabolizing enzymes and drug-transporting proteins are significantly altered in renal failure (9–12). In addition to the changes in pharmacokinetics and drug metabolism, the body's response to therapeutic compounds also appears to change under severe kidney dysfunction. For example, sensitivity of the central nervous system (CNS) to barbiturates and centrally acting muscle relaxants has been reported to increase in rats with experimentally induced renal failure (13,14). It was also revealed that renal failure potentiates the neurotoxicity of fluoroquinolones due to not only by elevating the plasma drug concentration, but also by increasing sensitivity of the CNS to the neurotoxic effects of drugs (15,16).

This increased CNS sensitivity is possibly related to a perturbation in electrolyte homeostasis in the CNS (17). In fact, there are some reports indicating that changes in the sodium concentration of cerebrospinal fluid (CSF) affect the expression of receptors like the angiotensin type 1A receptor, and this consequently influences various enzyme activities and/or the autonomic nervous system (18,19). In addition, a specialized Na^+ channel was recently identified in the anterior region of the third ventricle, which regulates neural activities by sensing changes in the sodium concentration of CSF (20,21). However, mechanisms underlying the increased CNS drug sensitivity caused by renal failure have not been fully elucidated, and few studies have examined whether electrolyte homeostasis is perturbed in renal failure.

[1] Graduate School of Medicine, Dentistry and Pharmaceutical Sciences, Okayama University, Tsushima-Naka, Okayama, 700-8530, Japan.
[2] To whom correspondence should be addressed. (e-mail: taiba@pharm.okayama-u.ac.jp)

As a first step to clarify the underlying mechanisms leading to this increased sensitivity, it is helpful to evaluate the effects of renal failure on the sodium concentration of CSF, but such evaluations are often hindered by difficulties in examining the CSF concentration *in vivo*. One of the approaches to overcome this is to use the microdialysis method (22). This approach enables us to continuously monitor the concentration of various substances in a target tissue without affecting the fluid's volume and composition using a tiny probe precisely embedded in it (23). In addition to this approach, application of the clinically utilized cationic element lithium to examine monovalent cation movement is worth considering. It is reported that some sodium transporters, such as the Na^+–K^+–$2Cl^-$ co-transporter and Na^+/H^+ exchanger, similarly recognize and transport lithium (24,25). Since these transporters are likely to play an important role in maintaining sodium concentration in the CSF (26–29), the perturbed sodium concentration in the CSF is probably detected by evaluating the lithium disposition.

With these considerations, we investigated the effects of renal failure on lithium disposition in rats with experimentally induced acute renal failure (ARF), in which the microdialysis probe was precisely placed in the lateral ventricles to monitor the lithium concentration of CSF. In addition, since there are various electrolyte transporters expressed in the choroid plexus to maintain the water and electrolyte balance of CSF (26,30,31), the effects of renal failure on their expressions were examined while focusing on the Na^+–K^+–$2Cl^-$ co-transporter (NKCC1) and the Na^+/H^+ exchanger (NHE1), which are largely expressed in the choroid plexus.

MATERIALS AND METHODS

Materials

Lithium chloride was obtained from Nacalai Tesque (Kyoto, Japan). Ringer's solution was prepared by dissolving 8.6 g of sodium chloride, 0.3 g of potassium chloride, and 0.33 g of calcium dichloride in 1 L of distilled water. Purified rabbit anti-rat NKCC1 and anti-rat NHE1 polyclonal antibodies were purchased from Chemicon (Temecula, CA, USA). Other chemicals were of the finest grade available from local distributors.

Animals

Male Wistar (clean) rats (220–250 g) were purchased from Japan SLC Inc. (Hamamatsu, Japan). They were housed at 20–25°C and 40–50% humidity on a 12-h light/dark cycle, and were allowed free access to a standard laboratory diet (MF, Oriental Yeast Co., Ltd., Tokyo, Japan) and water prior to the experiments. For the experiments with glycerol-induced ARF rats, rats were injected with 50% glycerol saline solution (10 ml/kg) in the left and right leg muscles after 24-h water deprivation (32). They were normally fed thereafter. These rats were used in experiments 24 or 48 h after glycerol treatment. They are hereafter referred to as ARF24 and ARF48, respectively, when necessary to mention the elapsed time after ARF induction. The development of renal failure was confirmed based on the serum creatinine concentration. The serum creatinine concentration was increased from 0.59±0.07 mg/dl before glycerol treatment to 3.24±0.19 and 4.02±0.65 mg/dl after treatment in ARF24 and ARF48 rats, respectively. All animal experiments were performed in accordance with the guidelines for animal experimentation of Okayama University.

Evaluation of Lithium Concentration Profile in Plasma

After being anesthetized with sodium pentobarbital (50 mg/kg, i.p.), each rat was fixed on its back. A total of 450 μl of lithium chloride solution was administered at a dose of 0.5 or 4 mmol/kg from the right femoral vein. A 150-μl blood sample was then taken from the cervical vein at 5, 20, 45, 75, 120, 240, and 360 min into a heparinized tube. The blood sample was centrifuged at 8,000×*g* for 10 min to collect a plasma specimen for lithium determination.

The lithium concentration profile of plasma was characterized in a model-dependent manner, in which the observed lithium concentration was fitted to the following equation with a nonlinear, least-squares method:

$$Cp(t) = Ae^{-\alpha t} + Be^{-\beta t} \quad (1)$$

where Cp(t) is the lithium concentration in plasma at time t. Total lithium clearance CL_{total} was calculated by the equation below:

$$CL_{total} = \frac{D}{\left(\frac{A}{\alpha} + \frac{B}{\beta}\right)} \quad (2)$$

where A, B, α, and β are parameters to be determined with Eq. 1. D is the lithium dose administered to rats (0.5 or 4 mmol/kg). When the area under the lithium concentration–time curve (AUC) in plasma was compared with that in CSF, its value was calculated with the trapezoidal rule until 6 h.

Evaluation of Lithium Concentration Profile in CSF

Prior to the experiment, the permeation coefficient of the microdialysis probe was determined *in vitro* (23). The microdialysis probe assembly equipped with a semi-permeable cellulose membrane (A-I-8, Eicom Co., Ltd., Kyoto, Japan) was immersed in Ringer's solution containing 7.2 mM (50 μg/ml) lithium (donor solution). The semi-permeable membrane was 1 mm in length and 200 μm in diameter, and its permeation threshold was 50 kDa. The inlet and outlet of the probe assembly were connected to a syringe infusion pump (CMA/102, CMA Microdialysis AB, Solna, Sweden) and a fraction collector (CMA/142, CMA Microdialysis AB, Solna, Sweden), respectively. To determine the permeation coefficient, the probe's lumen was perfused with Ringer's solution at a rate of 0.5 μl/min, and the perfusion effluent from the outlet was collected every 60 min until 6 h. The donor solution was collected at the midpoint of the collection interval. The permeation coefficient was determined as the concentration in the effluent compared to the donor solution, giving a value of 34.1±1.1%.

In the experiment, after being anesthetized with sodium pentobarbital, each rat was fixed on a stereotaxic instrument (Model SR-5N, Narishige, Tokyo, Japan). Its skull was exposed, and a hole 1 mm in diameter was opened by drilling

the skull carefully without damaging brain tissue. A guide cannula (AG-8, Eicom Co., Ltd., Kyoto, Japan) was then inserted into the brain tissue through the hole, and its tip was placed in the right lateral ventricle. The guide cannula was then fixed to the skull with a screw and dental cement. Subsequently, the microdialysis probe assembly was inserted into the ventricle through the guide cannula, and the tip of the assembly's semipermeable membrane was placed precisely at the following brain atlas coordinates originating from the bregma (33): anterior, 0.0 mm; lateral, 1.5 mm; ventral, 3.2 mm. The inlet and outlet of the probe assembly were connected to a syringe infusion pump (CMA/102) and a fraction collector (CMA/142), respectively, and the probe's lumen began to be perfused with Ringer's solution at a rate of 0.5 μl/min.

After a 1-h equilibration period, lithium chloride solution was administered into the right femoral vein at a dose of 4 mmol/kg. Effluent from the outlet was collected every 30 min until 6 h, and its lithium concentration was determined. The CSF lithium concentration at the midpoint of the collection interval was calculated with the determined concentration by taking into account the probe's permeation coefficient, described above. The AUC in CSF was calculated by the trapezoidal rule.

Lithium Determination

The lithium concentration was determined with an atomic absorption spectrometer at a wavelength of 670.8 nm with lithium standard solutions prepared at 1.44, 14.4, 36, 72, 108, 144, and 360 μM, in which coefficient of determination was larger than 0.995. Plasma specimens were diluted 20 or 50 times with distilled water for lithium determination. CSF specimens were added to distilled water to adjust their volume to 300 μl according to the manufacturer's instruction of the spectrometer, and then, the lithium concentration was determined. The determination was performed without repetition, because the volume of the specimen was insufficient for multiple determinations. The lowest lithium concentrations detectable in this study were 1.5 and 30 μM for the plasma and CSF specimens, respectively.

Evaluation of NKCC1 and NHE Expressions in the Choroid Plexus

A membrane fraction for the evaluation of choroid plexial NKCC1 and NHE1 expressions was prepared on two consecutive days, in which the membrane fraction from normal rats was prepared on day 1, and that from ARF rats was prepared on day 2. As for the preparation, each rat was fixed on its back after being anesthetized via diethyl ether inhalation. A midline incision was carefully made and the thoracic cavity was opened by cutting the ribs to expose the left and right carotid arteries. The rat was then sacrificed by cutting the vena cava. Immediately after, a 20-gauge needle attached to a syringe filled with 30-ml ice-cold saline was inserted into the carotid artery, and any blood remaining in the brain tissue was gently washed out. The whole brain was then excised, and horizontally cut to expose the lateral ventricles. Then, choroid plexial epithelia were collected under a magnifying glass (34). They were suspended in ice-cold, phosphate-buffered saline (PBS) followed by homogenization with 20 strokes at 500 rpm using a Teflon potter homogenizer. The homogenized specimen was subjected to conventional differential centrifugation (35): it was centrifuged at 9,000×*g* for 20 min, and the resultant supernatant was re-centrifuged at 105,000×*g* for 60 min. The obtained precipitate was re-suspended in PBS, and its protein content was determined with the Bradford method using a protein assay kit (Bio Rad, Hercules, CA, USA). The suspended membrane fraction was stored at −82°C.

NKCC1 and NHE1 expressions were evaluated using the Western immunoblot method (36). After 5-min boiling with 2-mercaptoethanol, the suspension of the membrane fraction was applied to an SDS-polyacrylamide (10%) gel at 4.2 or 5.0-μg protein/lane. The gel was subjected to 90-min electrophoresis followed by a transfer process to a nitrocellulose membrane. The membrane was then subjected to an overnight blocking process with 4% skim milk containing 0.4% Tween 20 at 4°C. After that, it was incubated for 1 h with the anti-NKCC1 or anti-NHE1 antibody diluted at 1:1,000. The migration pattern was visualized with the Vectastain Elite ABC Kit (Vector Laboratories, Burlingame, CA, USA) according to the manufacturer's instructions. The visualized band signals were semi-quantitatively analyzed based on densitometric readings.

Data Analysis

Data are shown as the means ± SE of three to nine experiments. Significant differences were evaluated by Student's *t* test, and $p<0.05$ was considered significant.

RESULTS

Effect of Acute Renal Failure on the Plasma Lithium Concentration Profile

The lithium concentration–time profile in plasma was firstly evaluated in rats. As shown in Fig. 1A, the plasma

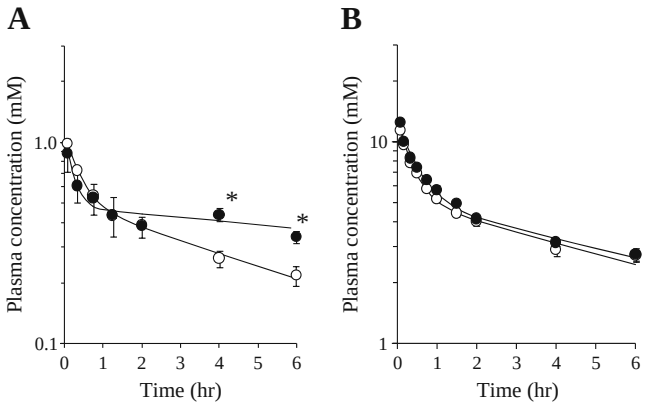

Fig. 1. Plasma concentration profiles of lithium at intravenous lithium doses of 0.5 (**A**) and 4 mmol/kg (**B**) in normal and ARF24 rats. *Solid lines* in both panels are the best-fit curves to the observed data, which were calculated with the nonlinear, least-squares method. The profiles in normal and ARF24 rats are indicated with *open* and *closed circles*, respectively. Data are shown as the mean ± SE of three to nine experiments. *Asterisk*, $p<0.05$: significantly different from the corresponding value in normal rats.

profiles following intravenous lithium administration at a dose of 0.5 mmol/kg were different between normal and ARF24 rats. The profile in ARF24 rats was reduced more slowly than that in normal rats, leading to the concentration in ARF24 rats being significantly higher in the terminal phase compared with that in normal rats (Fig. 1A). As a result, total lithium clearance in ARF24 rats was decreased to 20.8% of that in normal rats at a lithium dose of 0.5 mmol/kg (Table I). On the other hand, when experiments were performed at a lithium dose of 4 mmol/kg, no differences were observed in the profiles between normal and ARF24 rats (Fig. 1B). Model-dependent analysis also indicated that there were no differences in the concentration profiles between normal and ARF24 rats at a dose of 4 mmol/kg (Table I).

Effects of Acute Renal Failure on the CSF Lithium Concentration

The lithium concentration profile in CSF was then examined at an intravenous lithium dose of 4 mmol/kg, revealing that the concentration in CSF varied within a lower range, and declined at a slower rate compared with that in plasma in normal and ARF24 rats (Fig. 2). In addition, although the lithium concentration profiles in plasma were not different between normal and ARF24 rats, the CSF profile was revealed to be lower in ARF24 rats than that in normal rats (Fig. 2), resulting in the AUC of the CSF profile in ARF24 rats being significantly smaller than that in normal rats (Fig. 3). The lithium disposition to CSF was then evaluated as the AUC ratio between plasma and CSF, being 5.8±2.5% in ARF24 rats, which was 26.5% of that in normal rats (21.9±5.6%). The lithium disposition to CSF was also decreased in ARF48 rats, being 31.1% of the normal value (Fig. 3).

Effects of Acute Renal Failure on NKCC1 and NHE1 Expressions in the Choroid Plexus

To investigate the underlying mechanisms leading to the decreased CSF lithium concentration, NKCC1 and NHE1 expressions in the choroid plexus were evaluated in normal and ARF rats (Figs. 4 and 5). A significant increase of the NKCC1 expression was observed in ARF rats: expressions in ARF24 and ARF48 rats were 1.4 and 1.2-times greater than that in normal rats, respectively (Fig. 4A, B). As for the NHE1 expression, since two band signals were similarly detected, the total band density was evaluated and compared between normal and ARF rats (Fig. 5). As a result, the NHE1 expression was not different between normal and ARF rats.

DISCUSSION

To clarify the mechanism leading to increased CNS sensitivity when the renal function is seriously impaired, we evaluated the effects of renal failure on electrolyte homeostasis in CSF by examining lithium distribution. As shown in Fig. 2, the lithium concentration profile in CSF following intravenous lithium administration was significantly lower in ARF than in normal rats. It was also revealed that NKCC1 expression in the choroid plexus was increased in ARF rats, and this increased expression was similarly observed in ARF24 and ARF48 rats (Fig. 4). In contrast, the NHE1 expression was not altered in ARF rats (Fig. 5).

Maintaining water volume and electrolyte composition in CSF is crucial for the CNS to function normally. It is well-known that CSF is secreted at the choroid plexus, where various transporters and aquaporins are expressed and play important roles in controlling the electrolyte composition of CSF (26,30,31,37). Among those transporters, NKCC1 is one of the most predominantly expressed transporters on the apical side of the choroid plexus, and it contributes to regulation of the electrolyte concentration of CSF (27,28). Therefore, it is conceivable, in conjunction with our findings in this study, that electrolyte homeostasis in CSF is considerably perturbed when renal function is acutely impaired. This perturbation seems to be related to an altered NKCC1 expression in the choroid plexus (Fig. 4), which may result in sodium efflux from CSF to the blood. However, since the present study performed with ARF rats was not designed to clarify whether the increased NKCC1 expression is a cause of homeostasis perturbation or a response to the perturbation to maintain homeostasis, further investigations should be performed to elucidate the mechanisms via which electrolyte homeostasis in CSF is regulated in response to acute renal failure. In addition, it should be noted that lithium substitutes for sodium at selective transporters expressed in the choroid

Table I. Pharmacokinetic Parameters for the Plasma Concentration Profile of Lithium in Normal and ARF Rats Following Intravenous Lithium Administration at Doses of 0.5 and 4 mmol/kg

	0.5 mmol/kg		4 mmol/kg	
	Normal	ARF24	Normal	ARF24
Experiment[a]	3	3	9	4
Parameters[b]				
A (mM)	0.60±0.09	0.64±0.16	7.37±0.47	7.50±0.75
α (h^{-1})	2.61±0.36	4.94±1.84	2.66±0.28	2.12±0.87
B (mM)	0.51±0.05	0.48±0.14	4.94±0.23	5.11±0.70
β (h^{-1})	0.15±0.04	0.04±0.04	0.13±0.01	0.11±0.05
CL_{total} (ml h^{-1} kg^{-1})	132.0±23.0	27.5±27.0 [c]	88.1±11.2	78.3±20.2

[a] Data are shown as the means ± SE of three to nine experiments.
[b] Pharmacokinetic analysis was performed with the two-exponential equation described in "Materials and Methods" (see text).
[c] Significantly different from the corresponding value in the normal group ($p<0.05$)

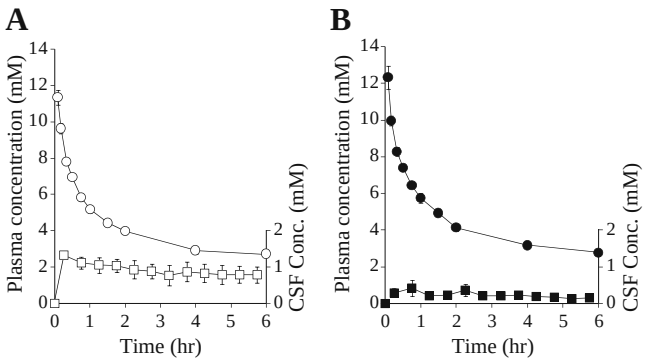

Fig. 2. Plasma and CSF concentration profiles of lithium in normal (**A**) and ARF24 rats (**B**) following intravenous lithium administration at a dose of 4 mmol/kg. The profiles in plasma and CSF are indicated with circles and squares, respectively. Data are shown as the mean ± SE of three to nine experiments.

plexus, and the effect of acute renal failure on the sodium concentration of CSF is necessary to be clarified in future study.

Although the altered CNS drug sensitivity observed with acute renal failure is unlikely to be explained only by an increased sodium efflux from CSF mediated by NKCC1, sodium concentration seems to be essential in regulatory mechanisms of CNS functions. In fact, it has been demonstrated that changes in sodium concentration in CSF, caused by infusing artificial, high-sodium CSF into the cerebral ventricle or administering a sodium-rich diet, led to sympathoexcitation and hypertension (38,39), and they modulate various gene expressions, such as for angiotensin-converting enzyme and angiotensin type 1A receptor (18,19). The existence of a specialized sodium channel which can sense a slight increase in the sodium concentration in CSF was also recently revealed (20,21). Further investigations will clarify the relationship between the CSF sodium concentration and CNS sensitivity to therapeutic compounds.

As for the increased NKCC1 expression observed in ARF rats, the precise mechanism responsible for this increase is currently unknown, but it can be speculated that the increased expression is partly related to an altered blood concentration of sex hormones induced by renal failure

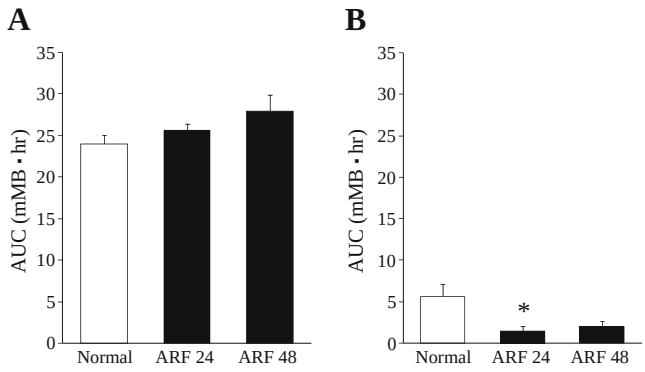

Fig. 3. Area under the lithium concentration–time curves (AUC) in plasma (**A**) and CSF (**B**) in normal and ARF rats. The AUC was calculated with the trapezoidal rule. Data are shown as the mean ± SE from three to nine experiments. *Asterisk*, $p<0.05$: significantly different from the value in normal rats.

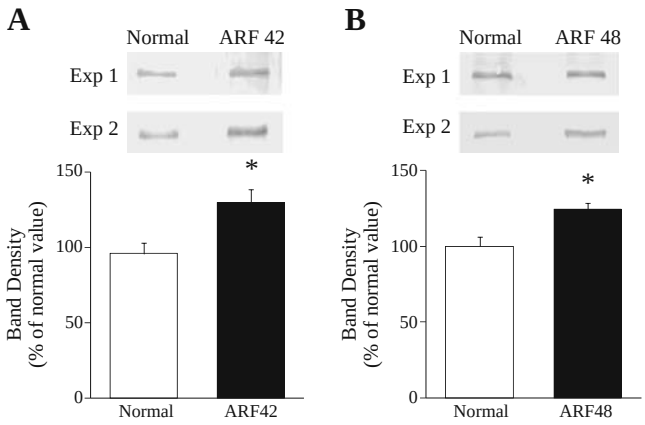

Fig. 4. Choroid plexial NKCC1 expression in normal and ARF rats. The expression was densitometrically quantified and shown as a bar graph with two representative results given on the Western immunoblot analysis. The membrane fraction of the choroid plexus was applied to an SDS-polyacrylamide (10%) gel at 4.2 (**A**) or 5.0 μg (**B**) of protein, and it was resolved by electrophoresis. Data are shown as the mean ± SE of four to eight experiments. *Asterisk*, $p<0.05$: significantly different from the value in normal rats.

(29,40,41), and the resultant imbalance in the protective properties of estrogens and the exacerbative properties of testosterone (42–44). In addition, it has been reported that NKCC1 expression is up-regulated by nerve growth factor (NGF) (45). Since NGF is known to be released in response to inflammation (46,47), it is likely that the ARF activates the

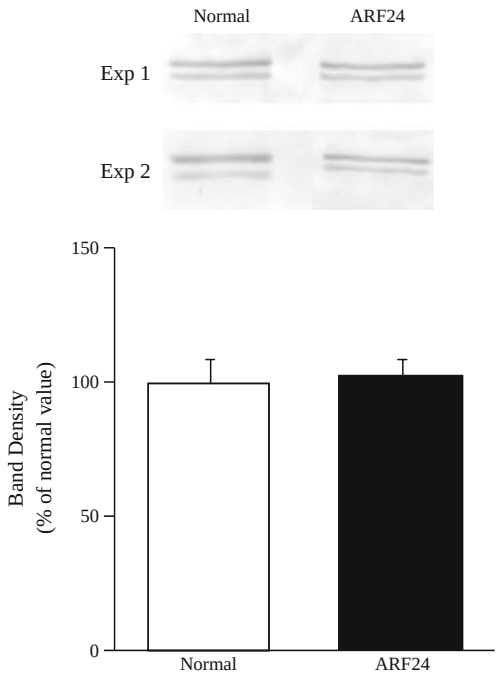

Fig. 5. Choroid plexial NHE1 expression in normal and ARF rats. Each of two band signals was densitometrically quantified and summed. The result was presented as a bar graph with two representative migration profiles given on the Western immunoblot analysis. The membrane fraction of the choroid plexus was applied to an SDS-polyacrylamide (10%) gel at 5.0 μg of protein. Data are shown as the mean ± SE of four experiments. No significance was detected between normal and ARF rats.

NGF-releasing process. NKCC1 expression may be facilitated by the released NGF stimulating the transcription of the NKCC1-encoding gene in ARF rats (48,49).

In this study, the plasma concentration profiles of lithium observed at a dose of 4 mmol/kg were the same between normal and ARF rats, while those observed at 0.5 mmol/kg were clearly different (Fig. 1 and Table I). The reason for this discrepancy is currently unknown, but since approximately 80% of lithium filtered at the glomerulus is reabsorbed in the proximal tubules (50), the saturation of some process involving lithium reabsorption may be related to the discrepancy. We performed experiments at a lithium dose of 4 mmol/kg (Fig. 2). This is because differences in the lithium concentration of CSF would be readily detected if its plasma profiles were the same between normal and ARF rats (Fig. 1B). In addition, the CSF lithium concentration needed to be raised high enough for its accurate determination. It is unlikely that the dose-dependency observed in the lithium plasma profile is related to our findings that the disposition of lithium to CSF is altered in ARF rats.

In summary, we demonstrated that the lithium concentration of CSF is decreased in ARF rats, and this reduction seemed to be accompanied by an increased NKCC1 expression in the choroid plexus. With these findings, electrolyte homeostasis in CSF is probably perturbed when renal function is seriously impaired, and this perturbation may be a reason why a change of CNS sensitivity to therapeutic compounds is caused by renal failure. Although the precise mechanisms underlying such altered CNS sensitivity still remain to be clarified, our findings will be helpful in providing optimal treatment for patients with renal failure.

ACKNOWLEDGEMENTS

This work was supported by a Grant-in-Aid for Scientific Research from the Japan Society for the Promotion of Sciences.

REFERENCES

1. J. Schnermann. Sodium transport deficiency and sodium balance in gene-targeted mice. *Acta. Physiol. Scand.* **173**:59–66 (2001).
2. D. Biemesderfer, J. Pizzonia, A. Abu-Alfa, M. Exner, R. Reilly, P. Igarashi, and P. S. Aronson. NHE3: a Na^+/H^+ exchanger isoform of renal brush border. *Am. J. Physiol.* **265**:F736–F742 (1993).
3. M. R. Kaplan, D. B. Mount, and E. Delpire. Molecular mechanisms of NaCl cotransport. *Annu. Rev. Physiol.* **58**:649–668 (1996).
4. H. Garty, and L. G. Palmer. Epithelial sodium channels: function, structure, and regulation. *Physiol. Rev.* **77**:359–396 (1997).
5. F. A. Leblond, L. Giroux, J. P. Villeneuve, and V. Pichette. Decreased *in vivo* metabolism of drugs in chronic renal failure. *Drug Metab. Dispos.* **28**:1317–1320 (2000).
6. Y. J. Moon, A. K. Lee, H. C. Chung, E. J. Kim, S. H. Kim, D. C. Lee, I. Lee, S. G. Kim, and M. G. Lee. Effects of acute renal failure on the pharmacokinetics of chlorzoxazone in rats. *Drug Metab. Dispos.* **31**:776–784 (2003).
7. T. Kimura, A. Kobayashi, M. Kobayashi, K. Numata, Y. Kawai, Y. Kurosaki, T. Nakayama, M. Mori, and M. Awai. Intestinal absorption of drugs in rats with glycerol-induced acute renal failure. *Chem. Pharm. Bull.* **36**:1847–1856 (1988).
8. H. Tanabe, S. Taira, M. Taguchi, and Y. Hashimoto. Pharmacokinetics and hepatic extraction of metoprolol in rats with glycerol-induced acute renal failure. *Biol. Pharm. Bull.* **30**:552–555 (2007).
9. F. A. Leblond, M. Petrucci, P. Dubé, G. Bernier, A. Bonnardeaux, and V. Pichette. Downregulation of intestinal cytochrome p450 in chronic renal failure. *J. Am. Soc. Nephrol.* **13**:1579–1585 (2002).
10. H. Sun, L. Frassetto, and L. Z. Benet. Effects of renal failure on drug transport and metabolism. *Pharmacol. Ther.* **109**:1–11 (2006).
11. Y. Masubuchi, M. Kawasaki, and T. Horie. Down-regulation of hepatic cytochrome P450 enzymes associated with cisplatin-induced acute renal failure in male rats. *Arch. Toxicol.* **80**:347–353 (2006).
12. J. Naud, J. Michaud, C. Boisvert, K. Desbiens, F. A. Leblond, A. Mitchell, C. Jones, A. Bonnardeaux, and V. Pichette. Down-regulation of intestinal drug transporters in chronic renal failure in rats. *J. Pharmacol. Exp. Ther.* **320**:978–985 (2007).
13. J. Dingemanse, M. Polhuijs, and M. Danhof. Altered pharmacokinetic- pharmacodynamic relationship of heptabarbital in experimental renal failure in rats. *J. Pharmacol. Exp. Ther.* **246**:371–376 (1988).
14. M. Yasuhara, and G. Levy. Kinetics of drug action in disease states. XXVII. Effect of experimental renal failure on the pharmacodynamics of zoxazolamine and chlorzoxazone. *J. Pharmacol. Exp. Ther.* **246**:165–169 (1988).
15. J. Kawakami, K. Ohashi, K. Yamamoto, Y. Sawada, and T. Iga. Effect of acute renal failure on neurotoxicity of enoxacin in rats. *Biol. Pharm. Bull.* **20**:931–934 (1997).
16. Y. Ishiwata, K. Son, Y. Itoga, and M. Yasuhara. Effects of acute renal failure and ganciclovir on the pharmacodynamics of levofloxacin-induced seizures in rats. *Biol. Pharm. Bull.* **30**:745–750 (2007).
17. M. Nagata, T. Fujichika, and M. Yasuhara. Effect of experimental renal failure and hypotonic hyponatremia on the pharmacodynamics of cefazolin-induced seizures in rats. *Pharm. Res.* **20**:937–942 (2003).
18. B. S. Huang, W. J. Cheung, H. Wang, J. Tan, R. A. White, and F. H. Leenen. Activation of brain renin–angiotensin–aldosterone system by central sodium in Wistar rats. *Am. J. Physiol. Heart Circ. Physiol.* **291**:H1109–H1117 (2006).
19. D. Mouginot, S. Laforest, and G. Drolet. Challenged sodium balance and expression of angiotensin type 1A receptor mRNA in the hypothalamus of Wistar and Dahl rat strains. *Regul. Pept.* **142**:44–51 (2007).
20. E. Watanabe, T. Y. Hiyama, H. Shimizu, R. Kodama, N. Hayashi, S. Miyata, Y. Yanagawa, K. Obata, and M. Noda. Sodium-level-sensitive sodium channel Na_x is expressed in glial laminate processes in the sensory circumventricular organs. *Am. J. Physiol. Regul. Integr. Comp. Physiol.* **290**:R568–R576 (2006).
21. S. N. Orlov, and A. A. Mongin. Salt-sensing mechanisms in blood pressure regulation and hypertension. *Am. J. Physiol. Heart Circ. Physiol.* **293**:H2039–H2053 (2007).
22. C. S. Chaurasia. *In vivo* microdialysis sampling: theory and applications. *Biomed. Chromatogr.* **13**:317–332 (1999).
23. Y. Kurosaki, M. Tagawa, A. Omoto, H. Suito, Y. Komori, H. Kawasaki, and T. Aiba. Evaluation of intramuscular lateral distribution profile of topically administered acetaminophen in rats. *Int. J. Pharm.* **343**:190–195 (2007).
24. S. Busch, B. C. Burckhardt, and W. Siffert. Expression of the human sodium/proton exchanger NHE-1 in *Xenopus laevis* oocytes enhances sodium/proton exchange activity and establishes sodium/lithium countertransport. *Pflügers Arch.* **429**:859–869 (1995).
25. R. T. Timmer, and J. M. Sands. Lithium intoxication. *J. Am. Soc. Nephrol.* **10**:666–674 (1999).
26. P. D. Brown, S. L. Davies, T. Speake, and I. D. Millar. Molecular mechanisms of cerebrospinal fluid production. *Neuroscience*. **129**:957–970 (2004).
27. M. D. Plotkin, M. R. Kaplan, L. N. Peterson, S. R. Gullans, S. C. Hebert, and E. Delpire. Expression of the Na^+–K^+–$2Cl^-$ cotransporter BSC2 in the nervous system. *Am. J. Physiol.* **272**: C173–C183 (1997).
28. Q. Wu, E. Delpire, S. C. Hebert, and K. Strange. Functional demonstration of Na^+–K^+–$2Cl^-$ cotransporter activity in isolated, polarized choroid plexus cells. *Am. J. Physiol.* **275**:C1565–H1572 (1998).

29. N. H. Nakamura, D. R. Rosell, K. T. Akama, and B. S. McEwen. Estrogen and ovariectomy regulate mRNA and protein of glutamic acid decarboxylases and cation–chloride cotransporters in the adult rat hippocampus. *Neuroendocrinology.* **80**:308–323 (2004).
30. Z. B. Redzic, J. E. Preston, J. A. Duncan, A. Chodobski, and J. Szmydynger-Chodobska. The choroid plexus–cerebrospinal fluid system: from development to aging. *Curr. Top Dev. Biol.* **71**:1–52 (2005).
31. J. Praetorius. Water and solute secretion by the choroid plexus. *Pflügers Arch.* **454**:1–18 (2007).
32. T. Aiba, M. Horiuchi, T. Makita, Y. Komori, H. Kawasaki, and Y. Kurosaki. Peritoneal dialysis alters tolbutamide pharmacokinetics in rats with experimental acute renal failure. *Drug Metab. Pharmacokinet.* **21**:291–296 (2006).
33. G. Paxinos, and C. Watson. *The Rat Brain in Stereotaxic Coordinates (2/e)*. Academic, New York, 1986.
34. R. D. Egleton, C. C. Campos, J. D. Huber, R. C. Brown, and T. P. Davis. Differential effects of diabetes on rat choroid plexus ion transporter expression. *Diabetes.* **52**:1496–1501 (2003).
35. T. Aiba, Y. Takehara, M. Okuno, and Y. Hashimoto. Poor correlation between intestinal and hepatic metabolic rates of CYP3A4 substrates in rats. *Pharm. Res.* **20**:745–748 (2003).
36. T. Aiba, M. Yoshinaga, K. Ishida, Y. Takehara, and Y. Hashimoto. Intestinal expression and metabolic activity of the CYP3A subfamily in female rats. *Biol. Pharm. Bull.* **28**:311–315 (2005).
37. V. A. Murphy, and C. E. Johanson. Na^+–H^+ exchange in choroid plexus and CSF in acute metabolic acidosis or alkalosis. *Am. J. Physiol.* **258**:F1528–F1537 (1990).
38. B. S. Huang, and F. H. Leenen. Brain amiloride-sensitive Phe-Met-Arg-Phe-NH_2-gated Na^+ channels and Na^+-induced sympathoexcitation and hypertension. *Hypertension.* **39**:557–561 (2002).
39. B. S. Huang, B. N. Van Vliet, and F. H. Leenen. Increases in CSF [Na^+] precede the increases in blood pressure in Dahl S rats and SHR on a high-salt diet. *Am. J. Physiol. Heart Circ. Physiol.* **287**: H1160–H1166 (2004).
40. T. S. Perrot-Sinal, C. J. Sinal, J. C. Reader, D. B. Speert, and M. M. McCarthy. Sex differences in the chloride cotransporters, NKCC1 and KCC2, in the developing hypothalamus. *J. Neuroendocrinol.* **19**:302–308 (2007).
41. L. Ji, S. Masuda, H. Saito, and K. Inui. Down-regulation of rat organic cation transporter rOCT2 by 5/6 nephrectomy. *Kidney Int.* **62**:514–524 (2002).
42. P. D. Metcalfe, and K. K. Meldrum. Sex differences and the role of sex steroids in renal injury. *J. Urol.* **176**:15–21 (2006).
43. S. E. Mulroney, C. Woda, M. Johnson, and C. Pesce. Gender differences in renal growth and function after uninephrectomy in adult rats. *Kidney Int.* **56**:944–953 (1999).
44. K. M. Park, J. I. Kim, Y. Ahn, A. J. Bonventre, and J. V. Bonventre. Testosterone is responsible for enhanced susceptibility of males to ischemic renal injury. *J. Biol. Chem.* **279**:52282–52292 (2004).
45. K. Nakajima, H. Miyazaki, N. Niisato, and Y. Marunaka. Essential role of NKCC1 in NGF-induced neurite outgrowth. *Biochem. Biophys. Res. Commun.* **359**:604–610 (2007).
46. H. Friess, Z. W. Zhu, F. F. di Mola, C. Kulli, H. U. Graber, A. Andren-Sandberg, A. Zimmermann, M. Korc, M. Reinshagen, and M. W. Büchler. Nerve growth factor and its high-affinity receptor in chronic pancreatitis. *Ann. Surg.* **230**:615–624 (1999).
47. K. Bielefeldt, N. Ozaki, and G. F. Gebhart. Role of nerve growth factor in modulation of gastric afferent neurons in the rat. *Am. Physiol. Gastrointest. Liver Physiol.* **284**:G499–G507 (2003).
48. N. E. Kremer, G. D'Arcangelo, S. M. Thomas, M. DeMarco, J. S. Brugge, and S. Halegoua. Signal transduction by nerve growth factor and fibroblast growth factor in PC12 cells requires a sequence of Src and Ras actions. *J. Cell Biol.* **115**:809–819 (1991).
49. T. Ito, T. Suzuki, and H. Ichinose. Nerve growth factor-induced expression of the GTP cyclohydrolase I gene via Ras/MEK pathway in PC12D cells. *J. Neurochem.* **95**:563–569 (2005).
50. M. D. Okusa, and L. J. Crystal. Clinical manifestations and management of acute lithium intoxication. *Am. J. Med.* **97**:383–389 (1994).